Yield stress determination in thixotropic crystal-melt suspensions

Kim Mishra[1], Damien Dufour[1], Silas Ehrengruber[1], Julia Merkel[1], and Erich J. Windhab[1]

[1]Institute of Food Nutrition and Health, ETH Zürich, Schmelzbergstrasse 9, 8092 Zürich

Crystal-melt suspensions (CMS) are yield stress shear thinning fluids in which crystal network formation is responsible for the appearance of a yield stress. This study investigates the influence of crystal concentration and morphology on the yield stress of CMS made from anhydrous milk fat (AMF), cocoa butter (CB), and palm kernel oil (PKO). Ultrasound veolocity profiling – pressure difference is applied to determine the yield stress directly after crystallization. Crystallization in laminar flow depends on shear, thus different shear rates are applied to produce CMS. For AMF and CB the yield stress decreases with increasing shear rate, whereas for PKO the opposite is the case. Polarized light microscopy (PLM) reveals that the change in crystal morphology as function of shear rate is responsible for the different behavior of AMF and CB compared to PKO. For AMF and CB, spherical (AMF) and needle (CB) like crystal aggregates are disaggregated with increasing shear rate leading to a weaker network. In the case of PKO, spherical are disaggregated into needle like crystal aggregates with increasing shear rate leading to an increased network formation.

Keywords: UVP-PD, rheology, crystal-melt suspension, yield stress, lipids and fats

1. Introduction

The flow behavior and material characterization of yield stress fluids containing crystals plays a major role in lipid (fat/oil), polymer, metal or magma melts as well as in concentrated solution/dispersion systems.[1]–[4] They have in common that a liquid (melt or solution) and solid (crystal) may coexist under given temperature conditions. From a rheological perspective, cooling a melt below its crystallization temperature or a solution below a temperature at which supersaturation reaches a critical value, crystal formation transforms the fluid system from a Newtonian fluid to a non-Newtonian suspension or even a semi-solid body. Rheology-structure relationships of crystallizing fluid systems are mostly quite complex since the crystal structure and formation kinetics can be altered by shear stress and related viscous friction-based energy dissipation acting in shear flow fields. Accordingly, thixotropy or rheopexy can be superimposed with related characteristic time scales depending on shear stress and energy dissipation rates as well as on the generated crystal shape and morphology. Such complex relationships are often poorly understood despite their relevance in applications of lipid, polymer, metal, or magma melt flow. Theoretical and experimental studies investigating lipid and magma melt rheology were found to reassemble each other.[4]–[6] Models proposed to describe lipid melts and magma systems do not contradict but rather complement each other in their different rheological description approaches. Lipid melts are characterized as weakly aggregated particle networks in the non-Newtonian shear flow regime, whereas magmas are treated as crystal-melt suspensions (CMS), with crystals interpenetrating each other described by the soft-core continuum percolation model.[4], [6], [7] The main difference between the two models is the derivation of a scaling factor α for the yield stress as a function of solids volume fraction and the presence/absence of a percolation threshold denoted as critical crystal fraction. For lipids, the fractal nature of the crystals is used to calculate such scaling factor α whereas for magmas the excluded volume of a given shape is used as calculation basis for α.[4], [6] The critical crystal fraction is calculated as function of crystal shape and defines the onset of a yield stress.[6]

In this paper, we investigated the rheological properties of CMS. Therefore, anhydrous milk fat (AMF), cocoa butter (CB), and palm kernel oil (PKO) were used as CMS model system. The liquid AMF, CB and PKO were transformed into a CMS with a scraped surface heat exchanger. Ultrasound velocity profiling - pressure difference (UVP-PD), polarized light microscopy, and pulsed nuclear magnetic resonance spectroscopy were employed to analyze and relate crystal volume fraction, crystal shape and crystal polymorphic form to the yield stress and viscosity of the CMS.

2. Material and Methods

PKO (RSPO-SG) was purchased from Florin AG (Muttenz, Switzerland). The PKO was fully molten overnight at 40 °C using a blade stirrer (RW 28W, IKA Werke GmbH, Staufen, Germany) before being used for trials.

Cocoa butter (CB) was kindly donated by Chocolat Frey AG (Buchs AG, Switzerland). Countries of origin are Nigeria, Cameroon, Ivory Coast and Ghana. The fatty acids were 61.5 wt\% saturated, 35 wt\% monounsaturated and 3.5 wt\% polyunsaturated. The CB was fully molten overnight at 45 °C using a blade stirrer (RW 28W, IKA Werke GmbH, Staufen, Germany) before being used for trials.

AMF was donated by Mibelle AG (Buchs, Switzerland). The AMF was fully molten overnight at 40 °C using a blade stirrer (RW 28W, IKA Werke GmbH, Staufen, Germany) before being used for trials.

Crystallization was performed with a scraped surface heat exchanger (SSHE) (Schröder GmbH & Co KG, Lübeck, Germany). The stator diameter $2R_o$ was 60 mm with a length of 400 mm. Using a MS25-HT/P water bath (Julabo Labortechnik GmbH, Seelbach, Germany) with 3.2 kW cooling capacity the double mantled stator was tempered within a temperature range of 5 – 18 °C. The rotor with two blades had a diameter $2R_i$ of 57 mm and was tempered at 27 - 32 °C with a Julabo F32 water bath (Julabo Labortechnik GmbH, Seelbach, Germany). The rotational speed of the rotor was adjusted by using a V-belt transmission. Since Reynolds numbers were calculated to be larger than 10 during crystallization, the shear rate $\dot{\gamma}_{SSHE}$ was calculated by solely considering the velocity field between rotor and stator as described previously:[8]–[10]

$$\dot{\gamma}_{SSHE} = \pi \frac{n_{SSHE}}{15} \frac{R_o^2}{R_o^2 - R_i^2}$$

where n_{SSHE} is the rotational speed, R_o the stator radius and R_i the rotor radius. An eccentric worm-drive pump (Allweiler GmbH, Radolfzell, Germany) pumped the liquid AMF, CB, and PKO from the double mantled stainless-steel vessel through double mantled and tempered 25 mm pipes into the gap between stator and rotor.

Solid fat content was measured by pulsed nuclear magnetic resonance spectroscopy using a 20 MHz (0.47 T) minispec mq20 (Bruker Biospin, Fällanden, Switzerland) in the direct mode. The device was calibrated using paraffin–acrylic standards. Tempered glass tubes with an inner diameter of 1 cm, a wall thickness of 0.06 cm and a height of 18 cm were filled with 3-4 cm of sample and immediately analyzed as described previously.[11] For highly viscous samples a tempered syringe with a plastic tube was used to fill the glass tubes. Analyses were performed in triplicate.

The UVP-PD measurements were done directly after crystallization. Double mantled 15 mm pipes held at 27 – 32 °C were used to convey the crystal-melt suspension. The pressure difference was measured in a 3.29 m pipe section. A diaphragm pressure sensor (CC1020, Labom GmbH, Hude, Germany) with a measurement range of 1.0 – 1.4 bar absolute pressure was used at the beginning of the pipe segment in order to calculate the pressure difference against atmospheric pressure at the pipe exit. In between the pressure sensor and the end of the pipe segment a custom-built polyvinyl chloride cell with inserted ultrasonic transducers was used to record the flow profile. Two 4 MHz transducers (Imasonic SAS, Voray-sur-L'Ognon, France) with an active diameter of 5 mm were placed at 60° and 90° angle with respect to the flow axis in order to determine the velocity profile across the pipe diameter and the speed of sound consecutively. The transducers were preferably operated at 3.75 MHz with a pulse repetition frequency of 750 Hz and 128 repetitions. The signals of the transducers were recorded with the UB-Lab device (Ubertone, Schiltigheim, France). During approximately 60 s a total of six averaged profiles were recorded for one process setting. This procedure was repeated three times for each process setting. Subsequently the profiles were deconvoluted[12]–[14] and fitted with the Herschel-Bulkley model. Fitting the Herschel-Bulkley model onto the measured velocity profile requires the plug radius R_p, flow index n and consistency factor K as fitting parameters:

$$\nu_x(r) = \begin{cases} \frac{n}{n+1} \frac{\Delta P}{2L_{pi}K}^{\frac{1}{n}} \left[(R_{pi} - R_{pl})^{1+\frac{1}{n}} - (r - R_{pl})^{1+\frac{1}{n}} \right], & \text{if } r \geq R_{pl} \\ \nu_x(R_{pl}), & \text{if } r < R_{pl} \end{cases}$$

The fitted plug radius R_p is related to the yield stress of the CMS as follows:

$$R_p = \frac{2\tau_0 L_p}{\Delta P}$$

Consequently, the larger R_p and ΔP the higher the yield stress τ_0 of the CMS. The illustration of the UVP-PD measurement track is

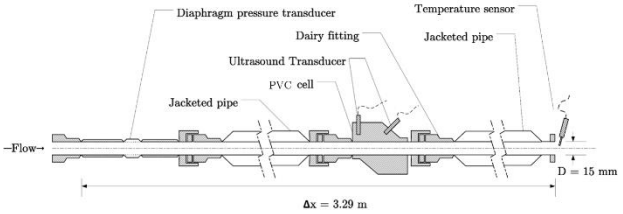

Figure 1: Schematic illustration of the UVP-PD measurement track

3. Results and Discussion

Figure 2 shows exemplarily pipe flow velocity profiles and back scattering amplitudes of CB CMS crystallized at $\dot{\gamma}_{SSHE} = 2150\ s^{-1}$ for varying crystal volume fractions Φ_{SFC}. It is evident that at low Φ_{SFC} an almost parabolic velocity profile is apparent as predicted by Newton's law. Already at $\Phi_{SFC} = 2.66\%$ a slight plug is evident indicating the onset of a yield stress. With further increasing Φ_{SFC} the plug extends to the pipe wall. At $\Phi_{SFC} = 8.80\%$, the plug extends almost the whole pipe radius denoting the upper yield stress limit at the given measurement conditions. At Φ_{SFC} of 1.73 and 2.66% the back scattering amplitude is small before increasing at intermediate Φ_{SFC} of 3.62 and 6.66%. At $\Phi_{SFC} = 8.80\%$ the backscattering amplitude rapidly decreases. For all crystal volume fractions, the far side of the transducer (positive r-coordinate) shows inaccurate velocity readings close to the pipe wall.

The small backscattering amplitude at low Φ_{SFC} is caused by insufficient number of particles for scattering. Contrary at high Φ_{SFC}, the crystals in the plug are not oriented in the flow field and are therefore increasing the attenuation coefficient leading to small backscattering amplitudes. The inaccurate velocity readings in the far side of the transducer were overcome by only considering the data from the near side of the transducer to calculate the viscosity data.

Figure 3 (A-C) shows the yield stress τ_0 as function of crystal volume fraction Φ_{SFC} for AMF, CB and PKO

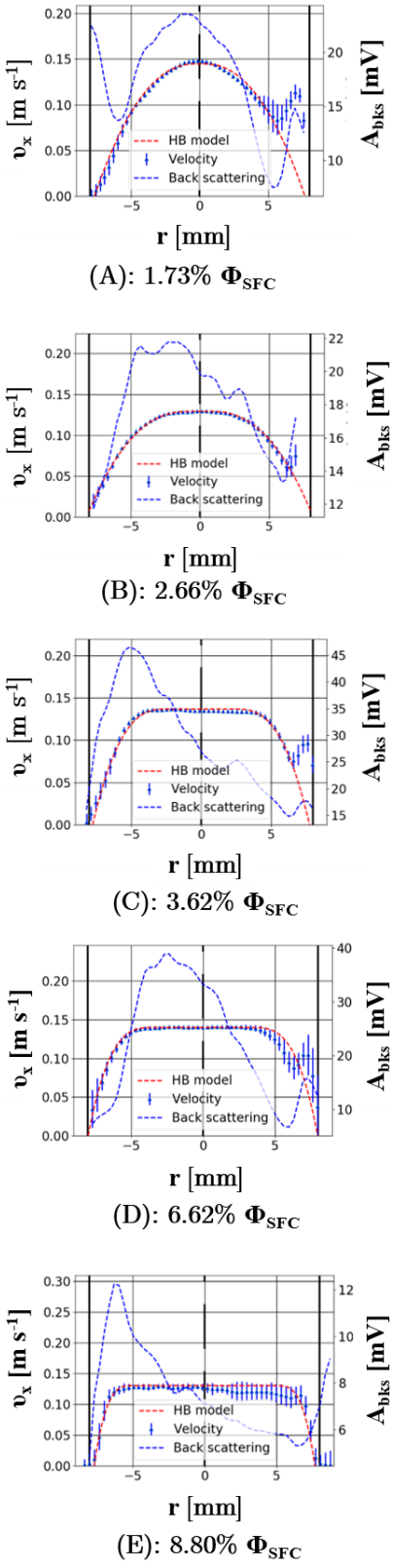

Figure 2: The fluid velocity in x-direction v_x on the left y-axis and the back scattering amplitude A_{bks} on the right y-axis as function of the pipe radius r for CB CMS crystallized at $\dot{\gamma}_{SSHE} = 2150\ s^{-1}$ for various crystal volume fractions Φ_{SFC}. The lines emerging from the velocity profile points indicate the magnitude of uncertainty. The dotted red line indicates the fitted velocity profile according to the model proposed by Herschel and Bulkley.

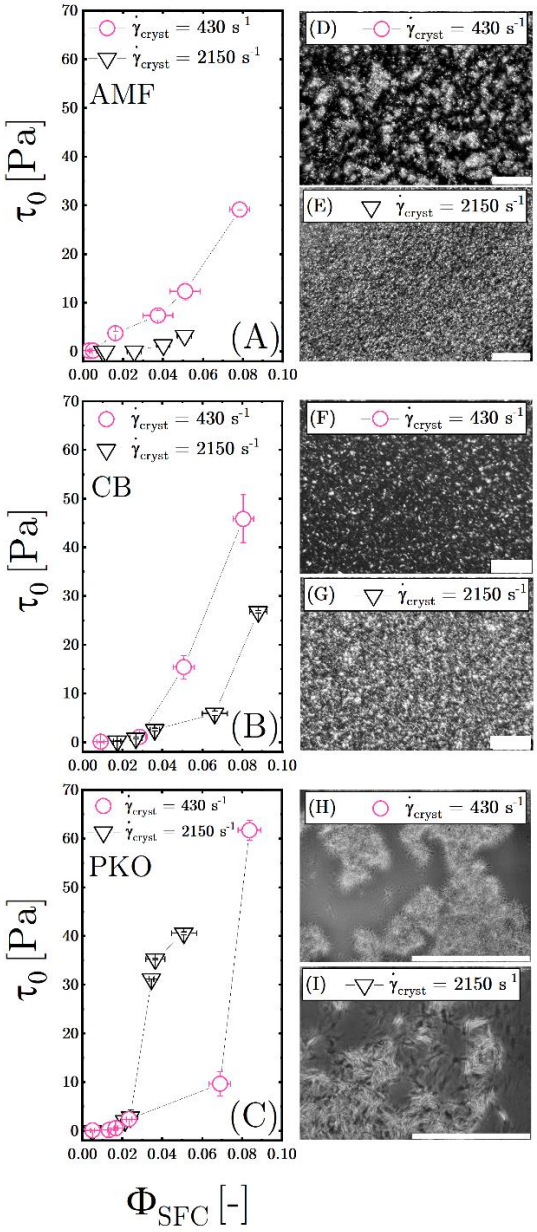

Figure 3: The yield stress τ_0 as function of the crystal volume fraction Φ_{SFC} for (A) AMF, (B) CB, and (C) PKO crystallized at $\dot{\gamma}_{SSHE} = 430\ s^{-1}$ and $\dot{\gamma}_{SSHE} = 2150\ s^{-1}$. (E-F) display polarized light microscopy images of the respective CMS for both crystallization shear rates. Bar represents 100 µm.

crystallized at $\dot{\gamma}_{SSHE} = 430\ s^{-1}$ and $\dot{\gamma}_{SSHE} = 2150\ s^{-1}$. For AMF and CB, the CMS crystallized at 430 s^{-1} shows a steeper τ_0 increase compared to the CMS crystallized at 2150 s^{-1}. For PKO, the opposite is the case. Furthermore, it is evident that AMF has lower absolute yield stresses compared to CB and PKO.

Figure 3 (E-J) show the corresponding polarized light microscopy images for AMF, CB, and PKO CMS crystallized at 430 and 2150 s^{-1}. At 430 s^{-1}, AMF shows spherical, large and loosely connected aggregates. At the same shear rate, CB shows small, isolated, and needle-like crystals. PKO shows spherulitic crystal aggregates at 430 s^{-1}, which are characterized by their spherical shape and brush-like surface. Increasing the shear rate to 2150 s^{-1},

AMF and CB crystals become smaller and less aggregated. For PKO however, the crystals change their shape from spherulitic to needle-like.

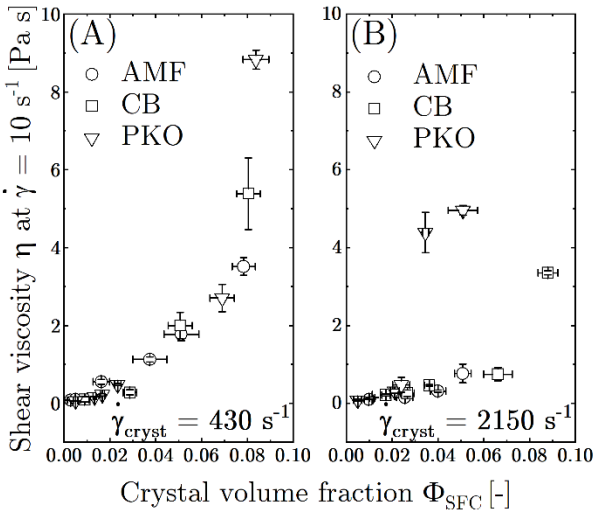

Figure 4: The shear viscosity measured at 10 s^{-1} $\eta_{\dot{\gamma}=10\,s^{-1}}$ as function of crystal volume fraction Φ_{SFC} for AMF, CB, and PKO crystallized at (A) 430 s^{-1}, and (B) 2150 s^{-1}.

Combining the information on the yield stress with the morphological insights from the polarized light microscopy images shows that AMF and CB CMS undergo a crystal deaggregation with increasing shear rates. Crystal morphology remains the same, however smaller crystals with fewer crystal-crystal bridges are present. For PKO a morphology change takes place with increasing shear rates. Spherical crystals turn into needle-like crystals. The needle-like crystals have a higher aspect ratio and therefore a decreased percolation threshold. Consequently, for PKO CMS crystallized at 2150 s^{-1} show a steeper increase of τ_0 as function of Φ_{SFC}.

Figure 4 shows the shear viscosity at 10 s^{-1} $\eta_{\dot{\gamma}=10\,s^{-1}}$ as function of crystal volume fraction Φ_{SFC} for AMF, CB, and PKO crystallized at (A) 430 s^{-1}, and (B) 2150 s^{-1}. Figure 4 (A) shows a mastercurve for the CMS viscosities crystallized at 430 s^{-1}. Below 3% Φ_{SFC}, a linear dependency between $\eta_{\dot{\gamma}=10\,s^{-1}}$ and Φ_{SFC} is apparent. Above 3% Φ_{SFC}, a non-linear increase characterizes the dependency of $\eta_{\dot{\gamma}=10\,s^{-1}}$ with Φ_{SFC} more accurately. Figure 4 (B) shows that AMF and CB crystallized at 2150 s^{-1} show decreased viscosities compared to 430 s^{-1} and a linear dependency of of $\eta_{\dot{\gamma}=10\,s^{-1}}$ with Φ_{SFC} up to 3% Φ_{SFC}. By contrast, PKO crystallized at 2150 s^{-1} shows an increased viscosity compared to 430 s^{-1}.

Figure 4 (A) shows that for CMS crystallized at 430 s^{-1}, crystal morphology does not affect the viscosity greatly. This can be explained by the increased importance of the crystal-crystal interactions due to aggregation. Figure 4 (B) shows that at 2150 s^{-1} crystal morphology affects the viscosity due to the deaggregation that takes place at such high shear rates. Consequently, the needle-like high-aspect ratio crystals of the PKO CMS result in higher viscosities compared to the lower aspect ratio AMF and CB crystals.

4. Conclusion

Measuring the rheological properties of crystal-melt suspensions (CMS) assists in understanding the flow and structure formation characteristics of liquid to semi solid polymer, metal, magma and lipid systems under crystallization conditions. The UVP-PD method was successfully employed to measure the influence of crystallization shear rate on the rheology of AMF, CB and PKO. Crystal volume fractions Φ_{SFC} up to 8.80% were measured accurately. This offers new possibilities to devise process control loops, which control for in-line real time data.

5. References

[1] A. R. McBirney and T. Murase, "Rheological properties of magmas," *Annu. Rev. Earth Planet. Sci.*, vol. 12, no. 1, pp. 337–357, 1984.

[2] O. Darras and R. Séguéla, "Tensile yield of polyethylene in relation to crystal thickness," *J. Polym. Sci. Part B Polym. Phys.*, vol. 31, no. 7, pp. 759–766, 1993.

[3] J. Banhart, H. Stanzick, L. Helfen, and T. Baumbach, "Metal foam evolution studied by synchrotron radioscopy," *Appl. Phys. Lett.*, vol. 78, no. 8, pp. 1152–1154, Feb. 2001.

[4] A. G. Marangoni and M. A. Rogers, "Structural basis for the yield stress in plastic disperse systems," *Appl. Phys. Lett.*, vol. 82, no. 19, pp. 3239–3241, 2003.

[5] S. R. Hoover, K. V. Cashman, and M. Manga, "The yield strength of subliquidus basalts - Experimental results," *J. Volcanol. Geotherm. Res.*, vol. 107, no. 1–3, pp. 1–18, 2001.

[6] M. O. Saar, M. Manga, K. V. Cashman, and S. Fremouw, "Numerical models of the onset of yield strength in crystal-melt suspensions," *Earth Planet. Sci. Lett.*, vol. 187, no. 3–4, pp. 367–379, 2001.

[7] M. O. Saar and M. Manga, "Continuum percolation for randomly oriented soft-core prisms," *Phys. Rev. E*, vol. 65, no. 5, p. 056131, May 2002.

[8] B. Breitschuh and E. J. Windhab, "Parameters influencing cocrystallization and polymorphism in milk fat," *J. Am. Oil Chem. Soc.*, 1998.

[9] E. Dumont, F. Fayolle, and J. Legrand, "Flow regimes and wall shear rates determination within a scraped surface heat exchanger," *J. Food Eng.*, vol. 45, no. 4, pp. 195–207, 2000.

[10] M. Stranzinger, A. Bieder, K. Feigl, and E. Windhab, "Effects of flow incidence and secondary mass flow rate on flow structuring contributions in scraped surface heat exchangers," *J. Food Process Eng.*, vol. 25, no. 3, pp. 159–187, Jul. 2002.

[11] B. Breitschuh and E. J. Windhab, "Direct measurement of thermal fat crystal properties for milk-fat fractionation," *J. Am. Oil Chem. Soc.*, vol. 73, no. 11, pp. 1603–1610, Nov. 1996.

[12] J. E. Jorgensen and J. L. Garbini, "An analytical procedure of calibration for the pulsed ultrasonic Doppler flow meter," *J. Fluids Eng.*, vol. 96, no. 2, pp. 158–167, Jun. 1974.

[13] P. Flaud, A. Bensalah, and P. Peronneau, "Deconvolution process in measurement of arterial velocity profiles via an ultrasonic pulsed Doppler velocimeter for evaluation of the wall shear rate," *Ultrasound Med. Biol.*, vol. 23, no. 3, pp. 425–436, Jan. 1997.

[14] M. Kagiyama, Y. Ogasawara, S. Tadaoka, and F. Kajiya, "Measurement accuracy of the flow velocity in pulsed ultrasound Doppler velocimeter," *Ultrasound Med. Biol.*, vol. 25, no. 8, pp. 1265–1274, Oct. 1999.